Propagation of 50 MHz radio waves in the *E*-layer

Mike Hasselbeck, WB2FKO

mph@sportscliche.com

First draft: 26 September 2025; Revised: 21 October 2025

Abstract

The propagation of 50 MHz radio waves in the E-layer is analyzed including refraction in realistic plasma gradients, Fresnel reflection, polarization, Earth curvature, and Faraday rotation. We show that the DX communication path is almost entirely determined by total internal reflection at path apex that occurs when the incidence angle reaches the critical angle. In the absence of ground gain, there is no advantage to the use of horizontally or vertically polarized antennas. Horizontal polarization is preferred, however, when ground reflection is involved.

Keywords: propagation, ionosphere, plasma, refraction, polarization, E-layer, 50 MHz

Introduction

Working 6-meter DX via sporadic-E propagation or meteor scatter requires reflection from ionized plasma. This ionization is present in the E-layer within the altitude range of approximately 80–150 km. The plasma density is highly variable as evidenced by dramatic daily, seasonal, and long-term solar-induced changes in VHF propagation. A simplified analysis ignores the curvature of the Earth and treats the ionosphere as a sheet of homogeneous plasma. Radio waves are assumed to travel in a straight path to this layer and reflect from a planar interface. Those constraints are removed here. A general ray-trace model is presented that is based on measured plasma profiles in the lower ionosphere.

It is generally accepted that there is no optimum antenna polarization for working VHF DX. Polarization is, however, an issue for moon-bounce (EME) particularly at 50 MHz because of Faraday rotation. This paper presents a detailed analysis using established physical principles to provide deeper insight on polarization and polarization rotation to aid in the operation of a high-performance amateur VHF station.

Ray tracing in the E-layer

Propagation is analyzed using standard ray trace techniques [1, 2]. The atmosphere is modeled as discrete, concentric shells i = 1, 2, 3... having refractive indices n_i as shown in Fig. 1. The layers have curvature that is parallel to the surface.

An antenna is located on the surface at height $h_0 = 0$ with radiation takeoff angle α_0 . For numerical analysis, it is convenient to set a fixed, incremental segment along the surface $\delta S = R_E \delta \beta$ where $R_E = 6378$ km is the radius of the Earth. The angle of incidence at each boundary is:

$$\theta_i = \frac{\pi}{2} - \alpha_i - \delta\beta \tag{1}$$

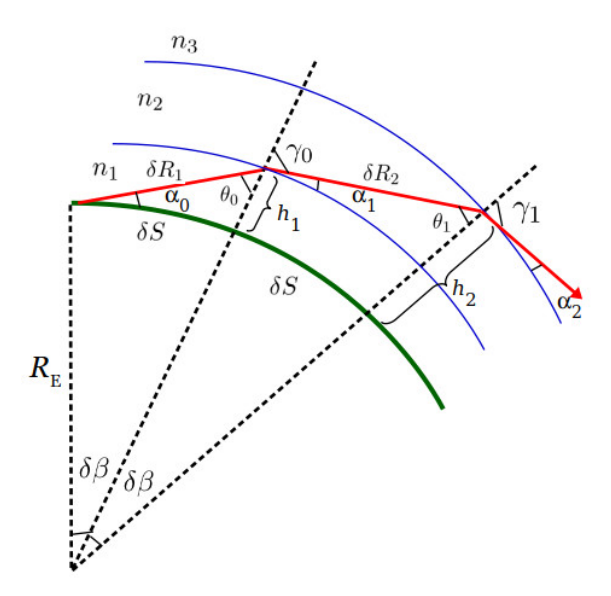


Figure 1: Ray tracing in vertically stratified refractive index layers with boundaries parallel to the Earth's surface.

The height of each interface boundary is found using the Law of Sines:

$$h_i = R_E \left[\left(1 + \frac{h_{i-1}}{R_E} \right) \frac{\sin(\alpha_{i-1} + \pi/2)}{\sin \theta_{i-1}} - 1 \right]$$
 (2)

The amount of refraction at each interface is obtained with Snell's Law:

$$n_i \sin \theta_{i-1} = n_{i+1} \sin \gamma_{i-1} \tag{3}$$

which sets:

$$\alpha_i = \frac{\pi}{2} - \gamma_{i-1} \tag{4}$$

The length of each incremental propagation segment is:

$$\delta R_i = (R_E + h_{i-1}) \frac{\sin \delta \beta}{\sin \theta_{i-1}} \tag{5}$$

The total electromagnetic path length is the sum of the segments: $\sum n_i \delta R_i$.

The condition of total internal reflection occurs when the incidence angle θ_{i-1} is greater than or equal to the critical angle θ' as defined by Snell's Law:

$$\frac{n_i}{n_{i+1}}\sin\theta' = 1\tag{6}$$

A critical angle may or may not exist, depending on the index difference at the boundary. Below the critical angle, partial reflections occur whenever there is a refractive index discontinuity. This can be calculated directly from the Fresnel formulas [3]. For horizontal polarization with interface at height h_i the reflectivity is:

$$\mathbf{R}_{i} = \left| \frac{n_{i} \cos \theta_{i-1} - n_{i+1} \cos \gamma_{i-1}}{n_{i} \cos \theta_{i-1} + n_{i+1} \cos \gamma_{i-1}} \right|^{2}$$
(7)

For vertically polarized waves:

$$\widetilde{\mathbf{R}}_{i} = \left| \frac{n_{i} \cos \gamma_{i-1} - n_{i+1} \cos \theta_{i-1}}{n_{i} \cos \gamma_{i-1} - n_{i+1} \cos \theta_{i-1}} \right|^{2}$$

$$(8)$$

The DX path length as measured along the surface of the Earth is the sum of the curved segments:

$$S = \sum \delta S = \sum R_E \delta \beta \tag{9}$$

It is important to emphasize that in vertically stratified index layers as we have here, no amount of refraction can return a wave to the surface. While refraction can alter the path trajectory, it is reflection that is essential for reversing the direction of the radio wave in the ionosphere.

Ionization in the layers is modeled as highly mobile electrons and a background of fixed, positively charged ions, i.e. a plasma. The refractive index of this dilute plasma is approximated as [3]:

$$n_i = \sqrt{1 - X_i} \tag{10a}$$

$$X_i = \kappa \frac{N_i}{f^2} \tag{10b}$$

where N_i is the plasma density (electrons or ions) in units of m⁻³, f is the frequency of the electromagnetic wave in Hz, and $\kappa = 80.43 \text{ J} \cdot \text{m/kg}$ is a physical constant.

Direct measurement of the plasma density in the E-layer is difficult. Continued improvements and refinements to experimental techniques, however, have led to better data and an evolving, semi-empirical model known as the Faraday International Reference Ionosphere [4]. In the altitude range 50 < h < 150 km, the density profile N(h) can be approximated as a double exponential, with two regions demarcated by a transition height h_k [5]:

$$N(h) = \begin{cases} 1.43 \times 10^{13} \exp(-0.15h') \exp\left[(\beta_D - 0.15)(h - h')\right] & \text{for } h < h_k \\ N(h_k) \exp\left[(\beta_E - 0.15)(h - h_k)\right] & \text{for } h_k < h < 150 \text{ km} \end{cases}$$
(11)

where h, h', and h_k are specified in km and N(h) is in units of m⁻³. The parameters have seasonal, latitude, and cyclical solar activity variations. For daylight hours, the data can be fit with h_k in the range 90–100 km, h'=65–75 km, $\beta_D=0.3$ –0.5 km⁻¹, and $\beta_E=0.14$ –0.17 km⁻¹.

In Fig. 2, three representative density profiles are plotted using Eq. (11) with $h_k = 95$ km and h' = 70 km. Low ionization density is obtained by setting $\beta_D = 0.35$ and $\beta_E = 0.17$ (dashed line); moderate ionization uses $\beta_D = 0.44$ and $\beta_E = 0.17$ (dotted line); high ionization has $\beta_D = 0.5$ and $\beta_E = 0.14$ (solid line). Note that exponential curves appear as straight lines on a logarithmic scale. The transition to a shallower gradient slope is clearly evident when $h > h_k$.

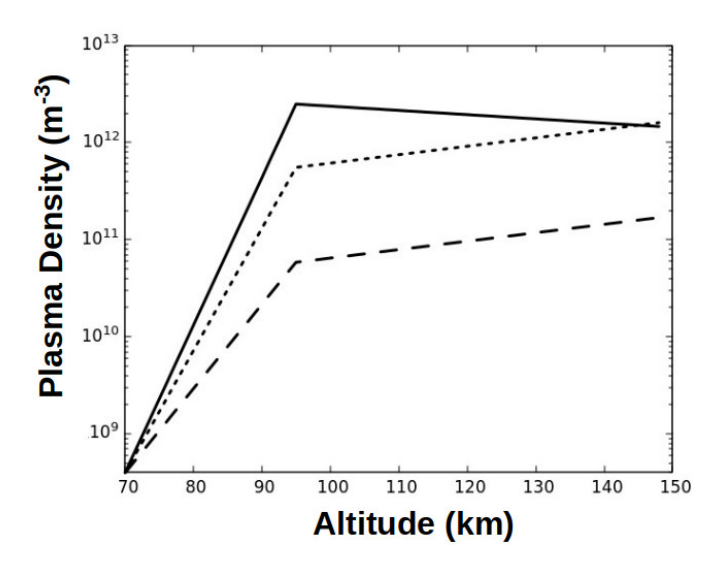


Figure 2: Three plasma density profiles in the E-layer as described in the text. Strong (solid line), moderate (dotted line), and weak ionization (dashed line).

The presence of the Earth's magnetic field in the E-layer induces left- and right-circular motion of free electrons due to the Lorentz force. This results in *birefringence*, i.e. the existence of two refractive indices that cause linearly polarized electromagnetic waves to become elliptically polarized [6]. This is sometimes referred to as Faraday rotation. To account for this magneto-ionic birefringence, Eq. (10) must be modified. The ordinary (n_o) and extraordinary (n_x) refractive indices are given by the Appleton-Hartree equation [7, 8]:

$$n_{o,x}^2 = 1 - \frac{2X_i(1 - X_i)}{2(1 - X_i) - Y_T^2 \pm \sqrt{Y_T^4 + 4(1 - X_i)^2 Y_L^2}}$$
(12)

where X_i is from Eq. (10b) and +/- refers to ordinary and extraordinary, respectively. The terms Y_L and Y_T are the longitudinal and tangential components of $Y = f_H/f$, respectively, where f_H is the magnetic gyro frequency. In the *E*-layer, $f_H = 1.4$ MHz [7, 8]. The angle ϑ between the propagation direction and magnetic field defines the two components: $Y_L = Y \cos \vartheta$ and $Y_T = Y \sin \vartheta$. Polarization rotation is maximum when $\vartheta = 0$ and minimum when $\vartheta = \pi/2$. Note that Eq. (10a) is recovered when Y = 0.

Results

We evaluate the path of 50 MHz radio waves as they traverse the E-layer density profiles of Fig. 2. Calculations are for two antenna takeoff angles $\alpha_0 = 3$ and 12 degrees using horizontal polarization. These angles represent the extrema of the primary radiation lobe on a typical weak-signal VHF antenna installation. For the moment, we ignore Faraday rotation.

Results for the low ionization profile (bottom curve in Fig. 2) are displayed in Fig. 3. The plasma density is insufficient to reflect the rays and they both escape at $h=150\,\mathrm{km}$. No DX communication path exists. Although there is negligible refraction, neither curve is a straight line. This is because altitude is plotted with respect to the Earth's surface, which is curving away from the straight ray path.

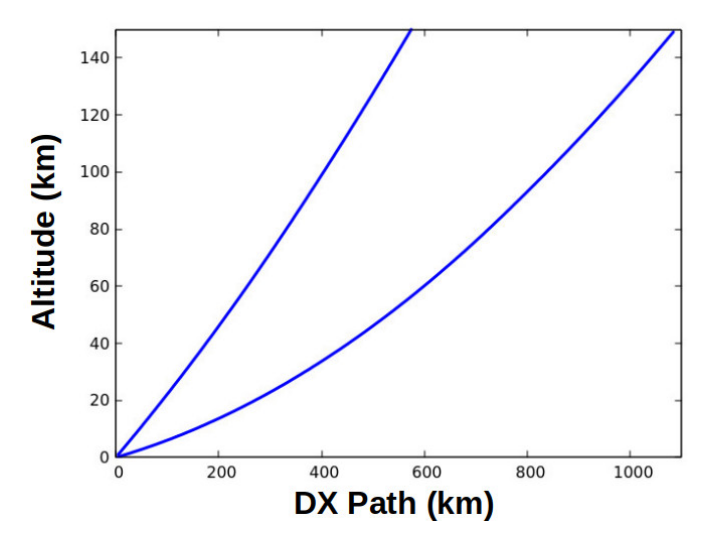


Figure 3: 50 MHz ray paths in a weakly ionized *E*-layer for $\alpha_0 = 3$ degrees (right curve) and $\alpha_0 = 12$ degrees (left curve). Neither ray is reflected.

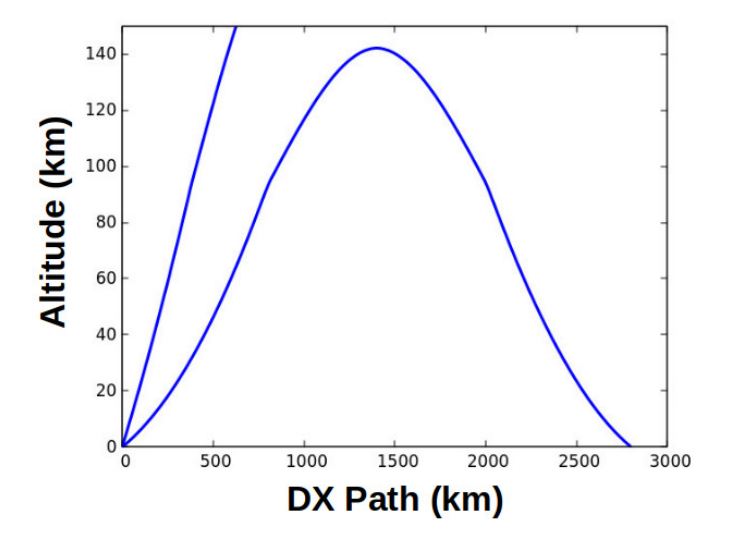


Figure 4: 50 MHz ray paths in a moderately ionized E-layer for $\alpha_0 = 3$ degrees (right curve) and $\alpha_0 = 12$ degrees (left curve).

The situation changes when the ionization density increases as described by the dotted curve in Fig. 2. Results for the same two takeoff angles are shown in Fig. 4. For $\alpha_0 = 3$ degrees, the critical angle is attained at h = 142 km and total internal reflection occurs. Fresnel reflection is negligible until just a few hundred meters below path apogee. A slight change of trajectory is visible at $h_k = 95$ km. The DX communication path is S = 2800 km. The ray launched at $\alpha_0 = 12$ degrees escapes.

When there is strong ionization (solid curve in Fig. 2) total internal reflection occurs for both antenna takeoff angles. Calculated ray trajectories are plotted in Fig. 5. Apogee is at h = 92 km for $\alpha_0 = 3$ degrees and h = 94 km for $\alpha_0 = 12$ degrees; the DX path is 1623 and 786 km, respectively. At this higher ionization density there is a dramatic reduction of S for $\alpha_0 = 3$ degrees because the wave is reflected at a lower altitude. This also explains why a decrease of the skip zone at 50 MHz is known to portend a potential opening on 144 MHz, although none of the density

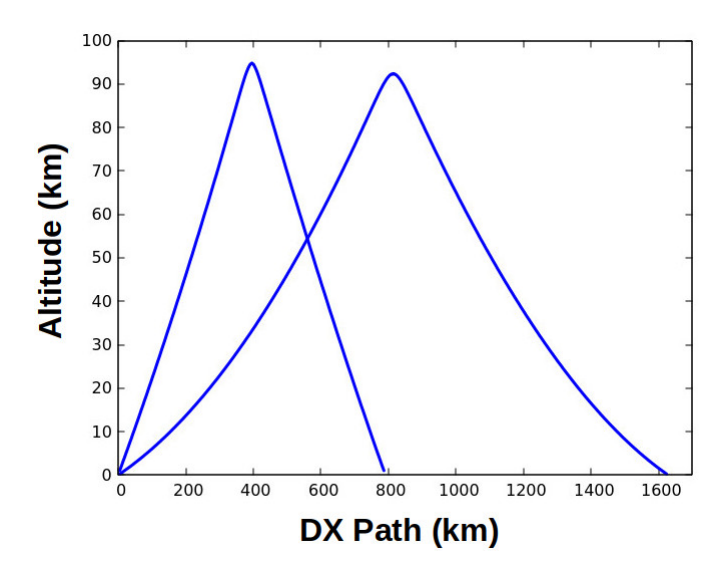


Figure 5: 50 MHz ray paths in a strongly ionized E-layer. Both rays experience total internal reflection.

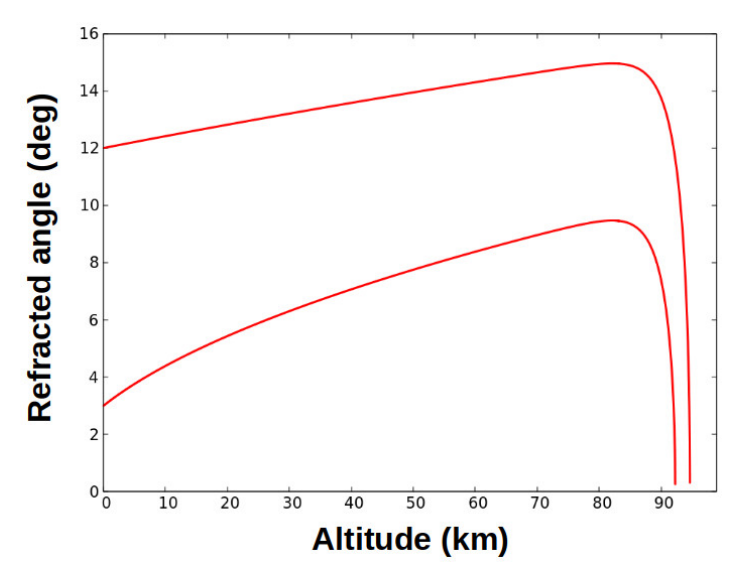


Figure 6: Refraction angle for the two antenna takeoff angles shown in Fig. 5. Upper curve: $\alpha_0 = 12$ deg; lower curve: $\alpha_0 = 3$ deg.

profiles considered here are sufficient to reflect signals on the higher frequency band.

Figure 6 plots the refraction angle (α_i in Fig. 1) as a function of altitude for the two curves in Fig. 5. At low altitudes (< 80 km), this angle is increasing entirely due to the sequence of curved interfaces since there is negligible refraction and the ray travels in a straight line. As refraction commences near the apex altitude, the angle decreases abruptly and total internal reflection occurs. There is a step-like increase in reflectivity from near zero to 100 percent.

Essentially identical results are obtained when comparing horizontal to vertical polarization (not shown). Reflection from the lower ionosphere is determined by the total internal reflection condition given by Eq. (6). The model reveals no advantage to using vertical polarized antennas for working VHF DX, either by sporadic-E propagation or meteor scatter.

To include magneto-ionic birefringence, the model is modified with n_o and then n_x in place of Eq. (10). There will be an accumulated phase shift arising from the difference in propagation path lengths for the ordinary and extraordinary rays:

$$\Delta \phi = \frac{2\pi f}{c} \left(\sum n_o \delta R_o - \sum n_x \delta R_x \right) \tag{13}$$

where c is the speed of light and the subscript i has been omitted for clarity. We find that the path lengths can differ by a kilometer or more, depending on antenna takeoff angle, ionization profile, and magnetic field orientation. These path differences (not shown) are a small percentage of the total path, but very large compared to the 6-meter radio wavelength. This means the phase difference $\Delta \phi$ can be expected anywhere in the range $0-2\pi$. The calculations confirm observations that linearly polarized 50 MHz signals will become elliptically polarized with random orientation upon reflection from the E-layer [6].

The ionization trail left by a meteor disintegrating in the E-layer will be radically different compared to the sporadic-E profiles shown in Fig. 2. We can expect a long, dense line of short-lived plasma of length 1 km or more and diameter of the order of 1 meter [10]. If ionization is greater than the critical density, the incident wave will be immediately reflected. Because the plasma cross-section is less than a wavelength, the polarization imparted by the transmitting antenna should be mostly preserved at the receiving point.

Ground gain

If the extended surface area in front of an elevated antenna (i.e. first Fresnel zone) is unobstructed and has reasonable conductivity, some ground gain can be expected. This is due to constructive interference of coherent radio waves, leading to a sequence of elevated lobes that produce the radiation pattern. For a flat, perfectly conducting surface, as much as 6 dB enhancement is possible.

Antenna modeling software is not transparent as to how it accounts for non-ideal ground. Insight can be obtained by calculating the reflectivity incorporating the permittivity of soil at VHF frequencies. The geometry is sketched in Fig. 7. Rays reflect from the ground at a distance d from the antenna mounted at height t, defining an angle $\tan(\pi/2 - \theta) = t/d$ with respect to the surface normal (dotted vertical line).

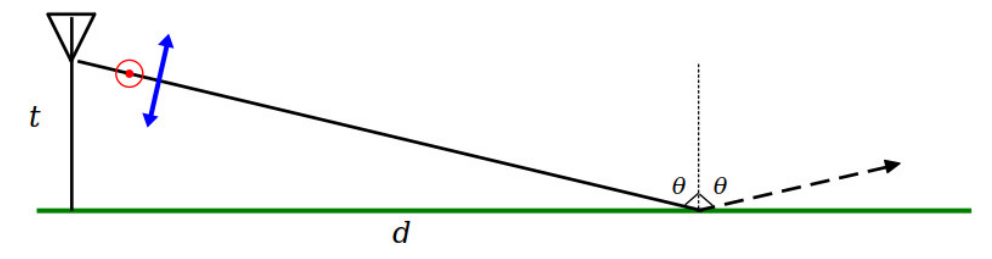


Figure 7: Linearly polarized waves from an antenna at height t strike the ground at distance d and angle θ . Horizontal polarization (red) has the electric field perpendicular to the plane of the page; vertical polarization depicts the E-field with the blue double-arrow.

Water content strongly affects soil conductivity and the corresponding dielectric constant, which is a complex quantity at VHF frequencies [9]. For dry, silty loam it is $\varepsilon = 4 + j$ whereas wet, silty clay

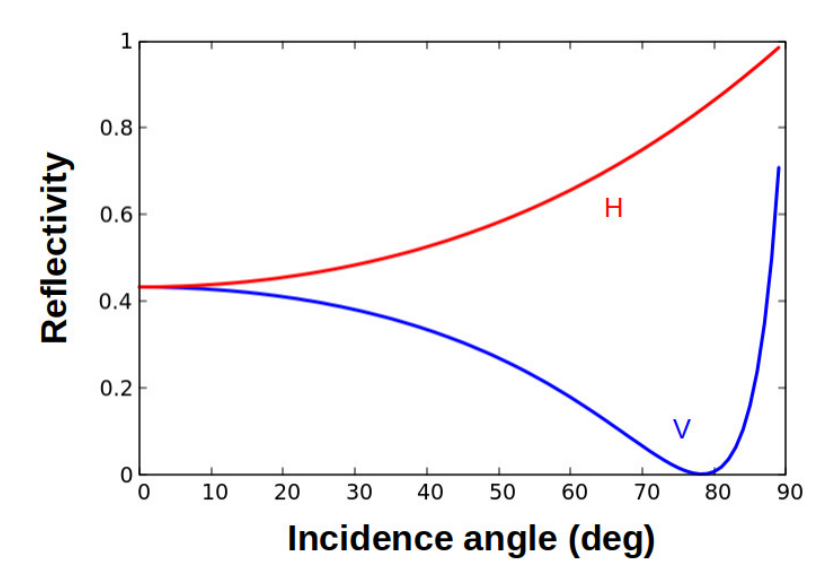


Figure 8: Calculated VHF reflectivity from wet, silty clay for horizontal polarization (H, red curve) and vertical polarization (V, blue curve). Soil permittivity is $\varepsilon_0(23+j2)$.

is approximately 23 + j2. When the dielectric constant is a complex number, the Fresnel equations become more complicated as shown in the Appendix [3].

Figure 8 plots the reflectivity of VHF rays as a function of the incidence angle (θ) for wet, silty clay with horizontal (H) and vertical (V) antenna polarizations. Complex soil permittivity is used in the calculation. The pronounced reflectivity null that occurs at around 78 degrees for vertical polarization is the well known pseudo-Brewster condition [11]. RF energy striking the ground around this angle will be absorbed and lost. For an antenna mounted at t=50 ft, this loss occurs over a broad area located 150–500 ft in front of the antenna. If ground gain is important, horizontal polarization is clearly more favorable.

Summary

Propagation of 50 MHz electromagnetic waves in the *E*-layer has been analyzed using ray-tracing with semi-empirical ionization profiles. We find that 100 percent reflection occurs abruptly at the critical angle. This is similar to light propagating in an optical fiber, although the ionosphere requires much shallower angles. The plasma density profile affects the altitude of the total internal reflection point and therefore the maximum DX path length. Very high ionization may severely limit single-hop 50 MHz propagation, but could also enable reflection on 144 and 222 MHz. The choice of antenna polarization is irrelevant *unless* it is desired to exploit ground gain to enhance the main radiation lobe. In that case, horizontal polarization should be preferred.

References

[1] B.R. Bean and E.J. Dutton, *Radio Meteorology* (NBS Monograph No. 92), National Bureau of Standards (1966).

- [2] Y. Zeng, U. Blahak, M. Neuper, and D. Jerger, "Radar Beam Tracing Methods Based on Atmospheric Refractive Index", J. Atmospheric and Ocean Technology **31**, 2650 (2014).
- [3] M. Born and E. Wolf, *Principles of Optics*, 6th ed., Pergamon Press: Oxford (1980).
- [4] M. Friedrich, C. Pock, and K. Torkar, "FIRI-2018, an Updated Empirical Model of the Lower Ionosphere", J. Geophysical Research: Space Physics 123, 6737 (2018).
- [5] W. Xu, R.A. Marshall, J. Bortnik, and J.W. Bonnell, "An Electron Density Model of the D- and E-Region Ionosphere for Transionospheric VLF Propagation", J. Geophysical Research: Space Physics 126, e2021JA029288 (2021).
- [6] C. Deacon, C. Mitchell, R. Watson, and B.A. Witvliet, "Evidence for the Magnetoionic Nature of Oblique VHF Reflections from Midlatitude Sporadic-E Layers", Atmosphere 13, 2027 (2022).
- [7] H. Rishbeth and O.K. Garriott, *Introduction to Ionospheric Physics*, Academic Press: NY (1969).
- [8] K.M. Yusupov and N.V. Bakhmetieva, "Sporadic E Layer with a Structure of Double Cusp in the Vertical Sounding Ionogram", Atmosphere 12, 1093 (2021).
- [9] Recommendation ITU-R P.527-4, "Electrical characteristics of the surface of the Earth" (2017).
- [10] M.M. Oppenheim and Y.S. Dimant, "First 3-D simulations of meteor plasma dynamics and turbulence", Geophysical Research Lett. **42**, 681 (2015).
- [11] R.J. Zavrel Jr, "Elevation and Pseudo-Brewster Angle Formation of Ground-Mounted Vertical Antennas", QEX, March/April (2016).

Acknowledgement. The author thanks J. Duffey KK6MC for helpful discussions and critical reading of the manuscript.

Updates to this document will be posted at: www.sportscliche.com/wb2fko/tech.html.

Appendix

The following formulation of the complex Fresnel equations is adapted from Ref. [3]. Consider an electromagnetic wave propagating from air $(\varepsilon_1 = 1)$ into soil having a complex dielectric constant ε_2 at angle θ as shown in Fig. 7. The dielectric constant of soil is:

$$\varepsilon_2 = \varepsilon' + j\varepsilon'' \tag{A.1}$$

Define the following two quantities:

$$2u^{2} = \varepsilon' - \sin^{2}\theta + \sqrt{[\varepsilon' - \sin^{2}\theta]^{2} + 4\varepsilon''^{2}}$$
(A.2)

$$2v^{2} = -\left[\varepsilon' - \sin^{2}\theta\right] + \sqrt{\left[\varepsilon' - \sin^{2}\theta\right]^{2} + 4\varepsilon''^{2}}$$
(A.3)

The reflectivity of a horizontally polarized wave is:

$$\mathbf{R}_{H} = \frac{(\cos \theta - u)^{2} + v^{2}}{(\cos \theta + u)^{2} + v^{2}}$$
(A.4)

and for vertical polarization:

$$\mathbf{R}_V = \frac{(\varepsilon' \cos \theta - u)^2 + (2\varepsilon'' \cos \theta - v)^2}{(\varepsilon' \cos \theta + u)^2 + (2\varepsilon'' \cos \theta + v)^2}$$
(A.5)

At normal incidence, $\theta = 0$ and the two polarizations are indistinguishable. Equations (A.4) and (A.5) must converge as is evident in Fig. 8.